Optical near-field photocurrent spectroscopy: A new technique for analyzing microscopic aging processes in optoelectronic devices

A. Richter, J. W. Tomm, and Ch. Lienau[a)]
Max-Born-Institut für Nichtlineare Optik und Kurzzeitspektroskopie, Rudower Chaussee 6, D-12489 Berlin, Germany

J. Luft
Siemens AG, Wernerwerkstrasse 2, D-93049 Regensburg, Germany

(Received 5 August 1996; accepted for publication 21 October 1996)

The potential of optical near-field photocurrent spectroscopy for analyzing microscopic aging processes in optoelectronic devices is demonstrated. The technique combines the subwavelength spatial resolution of near-field optics with tunable laser excitation, allowing for selective investigation of specific parts of the device structure. Experiments on GaAs/(AlGa)As high power laser diodes before and after accelerated aging provide direct visualization of defect growth within the *p-i-n* junction and information on aging-enhanced recombination processes close to the laser facet. The effect of wave guiding of the exciting light on the image formation is discussed. The nondestructiveness makes this technique a particularly attractive method for *in situ* analysis in high power laser diodes. © *1996 American Institute of Physics.* [S0003-6951(96)02252-8]

Aging processes of high-power laser diodes are of utmost importance for the performance and lifetime of the devices and have been investigated by a variety of techniques.[1,2] In this letter we describe and demonstrate a new analytical tool for monitoring microscopic aging processes in high-power laser diodes based on near-field photocurrent spectroscopy (NPCS). NPCS emerged as a new contrast method in near-field scanning optical microscopy.[3–5] In this technique, the near-field radiation transmitted through a nanometer-size aperture is used to generate photocarriers which induce a photocurrent inside the sample which basically acts as a photodiode. If the aperture is placed in close proximity to the sample, the excitation spot size is determined by the sub-wavelength sized of the aperture and can thus be reduced to below 50 nm. The resolution of the NPCS experiment is then determined by the excitation spot size, the absorption length of the radiation and minority carrier transport processes and could be shown to be better than 250 nm.[3] The technique presents several features that make it particularly attractive for the analysis of laser diodes. It combines high spatial resolution with nondestructiveness and the possibility of resonant excitation by using a tunable wavelength light source.

In our experiments, we investigated asymmetrically coated GaAs/(AlGa)As high power lasers. The double quantum well (DQW) graded index separate confinement heterostructure (GRINSCH) consists of a GaAs DQW (well width 10 nm) located in the center of two 220 nm wide undoped $Al_{1-x}Ga_xAs$ ($0.3<x<0.6$) graded gap layers.[6] This structure is surrounded by *n*- and *p*-doped 1.5–2 μm thick $Al_{0.6}Ga_{0.4}As$ cladding layers with an energy gap (E_g) of about 2.2 eV. The front facet reflectivity of about 5% was adjusted by a 120 nm thick Al_2O_3 layer. The photon energy of the laser emission of all devices was $\hbar\omega=1.53$ eV ($\lambda=808$ nm). For a fresh device threshold currents were in the order of 0.5 A and output powers were in the order of $P=1250$ mW at 2 A. Accelerated aging was realized at 35 °C for 100 h with an operation current of 1.75 A. The aging procedure and the changes of the device parameters are discussed in greater detail elsewhere.[7]

In the near-field photocurrent (NPC) experiments, the laser diode is excited by light transmitted through a nanometer-sized aperture at the end of a suitable near-field optical microscope probe tip. The photoinduced current (or voltage) across the *p-i-n* junction is then detected as a function of the tip position as the tip is scanned across the diode facet. During the scan the tip to sample separation is kept constant at 5 ± 1 nm using an optical shear-force setup[8] for distance regulation. Shear-force images of the surface topography are recorded simultaneously with the NPC images, providing a spatial correlation with an accuracy of 100 nm between the NPC signal and the layer structure of the laser diode being vital for interpretation of the experimental results. The fiber probe consists of a tapered single mode optical fiber (3M, 820 nm) with a lateral metal coating and a nanometer-sized aperture at its very tip.[9] Here, the aperture size was varied between 50 and 200 nm. Tunable continuous wave laser sources were used for excitation. The excitation light was amplitude-modulated at 1 kHz and the photoinduced signal was detected with a lock-in amplifier with the laser diode unbiased.

A macroscopic photocurrent (PC) spectrum (in arbitrary units, full circles) for a fresh laser device is depicted in Fig. 1. The calculated spectral shapes of the absorption edge [$\alpha_{\mathrm{DQW}}(\hbar\omega)$] of the DQW and $\alpha_{\mathrm{GRIN}}(\hbar\omega)$ of the bottom of the GRIN structure are added as full and dotted lines (in cm^{-1}), respectively.[10] The spectral shape of the PC spectrum is closely connected to the absorption coefficient of the whole structure. For all spectral positions the PC signal magnitude correlates with the sum $\Sigma\alpha_i(\hbar\omega)$ of the contributions (see Fig. 1) from the different layers (i). Furthermore, it depends on the gradient of the sum potential consisting of contributions of the band edges and the doping profile.

Three characteristic contributions to the PC spectrum are

a)Corresponding author. Electronic mail: lienau@mbi.fta.berlin.de

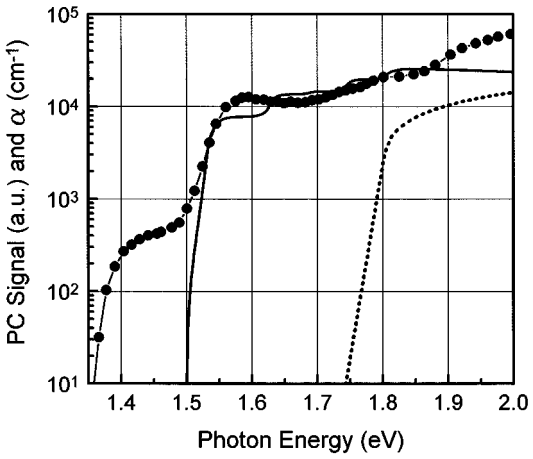

FIG. 1. Room-temperature macroscopic photocurrent (PC) spectrum (full circles, in a.u.) of a fresh high power laser diode. The calculated absorption coefficients (in cm^{-1}) of the DQW and the bottom of the GRIN region are depicted as full and dotted lines, respectively.

resolved. At excitation energies between 1.3 and 1.5 eV, i.e., below the effective band gap of the DQW structure of 1.53 eV, a weak shoulder in the spectrum is related to defect or impurity absorption. The strong signal increase at energies above 1.5 eV results from the onset of the interband absorption on the $1hh \rightarrow 1e$ transition from the first heavy hole to the first electron subband in the DQW (solid line). The reverse transition is responsible for the laser emission. At energies above 1.75 eV absorption by the graded gap layers sets in (dotted line) and this causes another increase in signal intensity.

Two-dimensional NPC images obtained from the same device recorded for different excitation energies are presented in Fig. 2(a). The images have been recorded with fiber probes with an aperture diameter of about 250 nm. The presented images are representative examples of a full set of images recorded at about 20 different spectral positions in the range between 1.44 and 1.965 eV. In Fig. 2(b), cross-sections through these images along a line perpendicular to the DQW plane are related to the laser diode structure. The wavelength dependence of the integrated intensity in these images follows roughly the macroscopic PC spectrum of Fig. 1. At 1.476 eV in the range of the impurity absorption, we observe a narrow NPC signal with a width of 700 nm and a maximum in the DQW region. At higher photon energies, the signal changes into a double maximum structure around the GRIN region and the active region of the laser now appears as a small dip in the center of this structure. The width of the structure is about 1 μm and the two peaks are separated by 450 nm. At 1.579 eV, we observe a signal background for excitation in the cladding layers and this background increases with increasing energy to about 60% of the maximum NPC signal at 1.959 eV.

The NPC data were analyzed by beam propagation calculations in order to understand the physical mechanisms underlying the image formation process. The propagation of the excitation light within the device was simulated by modeling the light field through the tip as a superposition of propagating and evanescent waves and considering the layer-specific absorption of each wave. Details will be given elsewhere, together with NPC studies of different laser structures.[11] The simulations showed that the contribution of waves which are evanescent inside the sample, to the NPC images are of minor importance for our structure. This is a result of the rather thick coating. At excitation energies below 1.49 eV, the NPC signal arises only from carriers generated through the absorption of impurity levels. The absorption coefficient of these impurity levels is small, so that the signal is dominated by waves guided inside the GRIN regions. For these guided waves, the effective absorption length is much longer than for unguided waves and they thus create a larger amount of carriers inside the *p-i-n* region. This directly explains the high spatial resolution of the NPC signal even though the signal is generated by weakly absorbed propagating waves. Due to the waveguiding effect inside the *p-i-n* region, the NPC signals in this diode are only weakly affected by minority carrier transport. At higher excitation energies, where absorption by the DQW region sets in, an increase in absorption coefficient, number of photogenerated carriers and thus NPC signal intensity is expected and observed. The pronounced double maximum shape of the NPC signal is, however, surprising. It can be attributed to a nonradiative (near-) surface recombination process. Its effect on the NPC image formation process can best be visualized by treating the tip as a point light source. Waves that are generated if the tip is located inside the DQW region experience a stronger wave guiding than those generated for tip locations inside the GRIN region. The difference in waveguiding leads to a variation in penetration depth of the guided waves with tip position. Carrier generation thus oc-

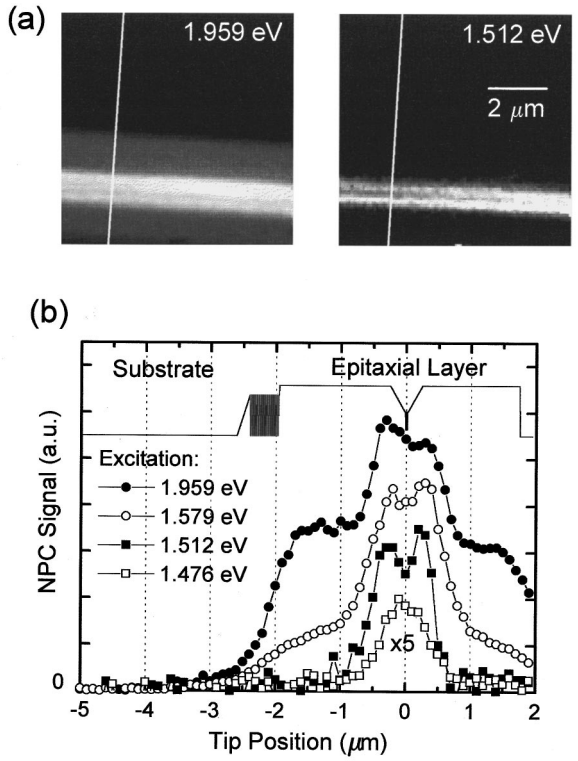

FIG. 2. (a) NPC images of a fresh DQW laser diode for different excitation energies of 1.512 and 1.959 eV. The photoinduced voltage across the *p-i-n* junction is mapped as a function of the position of the fiber tip. (Here, white regions are regions of a high NPC signal.) (b) NPC line scans of the same fresh diode. The shape of the conduction band potential is added (solid line).

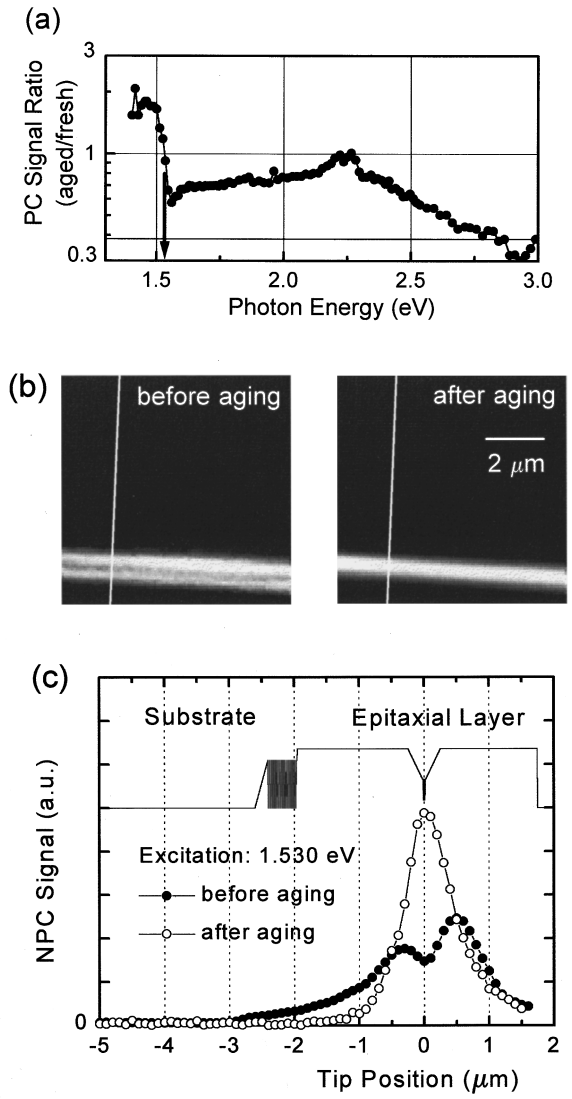

FIG. 3. PC and NPC data from a diode laser before and after an accelerated aging test. (a) Ratio of the PC signals after and before the aging test. (b) NPC images of the laser diode before and after the aging process at an excitation energy of 1.530 eV. The photoinduced voltage across the *p-i-n* junction is mapped as a function of the position of the fiber tip. (c) NPC line scans before and after aging measured at 1.53 eV.

curs closer to the surface if the tip is located inside the DQW. These carriers are more strongly affected by near-to-surface recombination processes and this leads to a smaller NPC signal. This interpretation is stongly supported by our beam propagation analysis. With increasing excitation energy, the absorption coefficient becomes large enough that unguided waves are also significantly absorbed inside or close to the GRIN–DQW region. This contribution from unguided waves gives rise to the increasing NPC background for high energy excitation (1.579 and 1.959 eV).

Bearing this knowledge in mind, we performed accelerated aging experiments. The combination of microscopic and macroscopic PC techniques provides a direct calibration of the absolute values of the NPC signals if one intends to compare NPC results obtained from different lasers or from one laser at different stages of aging. On the other hand, the NPC measurements give evidence about the local assignment of the structures in the PC spectrum. Figure 3(a) displays the ratio of the macroscopic PC spectra after and before aging. Obviously the impurity contributions are increased by the aging procedure whereas the DQW contribution reduced. Such aging fingerprints have been monitored several times for different diodes and different diode structures and can be considered to be typical for a given laser structure. Note, that the cladding layer with $E_g = 2.2$ eV seems to be less affected by the aging. The decrease of PC in the 2.3–3.0 eV region is caused by increased surface recombination. For the direct monitoring of the aging of this diode laser an excitation energy of 1.530 eV was chosen [see arrow in Fig. 3(a)] since there the integral of the NPC signal should not change. Such a behavior was found indeed in the NPC experiment displayed in Fig. 3(b). The double structure in the scan [c.f. Fig. 3(c)] taken from the fresh diode results from DQW absorption and waveguiding within the GRIN layer, as discussed above (c.f. Fig. 2). For the aged structure the double structure vanishes nearly completely indicating a reduction of the DQW contribution. The creation of defects is directly evident from the growth of the peak which is located *in center* of the junction. So far our discussion has not involved the nature of the defect accompanied to the aging. Preliminary macroscopic PC results extended to the infrared region allow to speculate that the defect monitored here is related to dislocations, which are known to be infrared active. This will be the subject of further investigations.

In summary, we presented the first combined study employing NPC and conventional PC at laser diodes for different stages of aging. We demonstrated that NPCS has the potential to provide direct insight into the microscopic processes of aging-induced defect creation and surface recombination in the active region of the laser diode.

The authors would like to thank A. Bärwolff, P. Enders, and U. Menzel for helpful discussions and Ch. Lier for expert technical assistance. Special thanks are due to T. Elsaesser for careful reading of the manuscipt and continuous support of this work.

[1] M. Fukuda, *Reliability and Degradation of Semiconductor Lasers and LEDs* (Artech House, Inc., Boston, 1991).
[2] P. G. Eliseev, *Reliability Problems of Semiconductor Lasers* (Nova Science, Commack, NY, 1991).
[3] S. K. Buratto, J. W. P. Hsu, E. Betzig, J. K. Trautman, R. B. Bylsma, C. C. Bahr, and M. J. Cardillo, Appl. Phys. Lett. **65**, 2654 (1994).
[4] M. S. Ünlü, B. B. Goldberg, W. D. Herzog, D. Sun, and E. Towe, Appl. Phys. Lett. **67**, 1862 (1995).
[5] B. B. Goldberg, M. S. Ünlü, W. D. Herzog, H. F. Ghami, and E. Towe, IEEE J. Selected Topics Quantum Electron **1**, 1073 (1995).
[6] M. Voss, C. Lier, U. Menzel, A. Bärwolff, and T. Elsaesser, J. Appl. Phys. **79**, 1170 (1996).
[7] J. W. Tomm, A. Bärwolff, U. Menzel, M. Voβ, R. Puchert, Th. Elsaesser, F. X. Daiminger, S. Heinemann, and J. Luft (unpublished).
[8] P. C. Yang, Y. Chen, and M. Vaez-Irvani, J. Appl. Phys. **71**, 2499 (1992).
[9] Ch. Lienau, A. Richter, and T. Elsaesser, Appl. Phys. Lett. **69**, 325 (1996).
[10] U. Menzel (unpublished).
[11] Ch. Lienau, A. Richter, and J. W. Tomm (unpublished).